Field-free line formation in a magnetic field

2010 J. Phys. A: Math. Theor. 43 012002

(http://iopscience.iop.org/1751-8121/43/1/012002)

IOP FTC
IOP PUBLISHING JOURNAL OF PHYSICS A: MATHEMATICAL AND THEORETICAL

J. Phys. A: Math. Theor. **43** (2010) 012002 (9pp) doi:10.1088/1751-8113/43/1/012002

FAST TRACK COMMUNICATION

Field-free line formation in a magnetic field

T Knopp, T F Sattel, S Biederer and T M Buzug

Institute of Medical Engineering, University of Lübeck, Lübeck, Germany

E-mail: knopp@imt.uni-luebeck.de

Received 9 September 2009, in final form 16 November 2009
Published 8 December 2009
Online at stacks.iop.org/JPhysA/43/012002

Abstract
In this communication, the theory of field-free line (FFL) formation in a magnetic field is investigated. It is shown that an FFL can be generated by only three Maxwell coil pairs. By varying the applied currents, the FFL can be arbitrarily rotated, while keeping the coils static in space. For translation, additional Helmholtz coil pairs can be used. These findings enable efficient realization of a field generating unit for a recently developed imaging method named magnetic particle imaging.

PACS numbers: 87.50.C−, 41.20.−q

1. Introduction

Magnetic particle imaging (MPI) is a new imaging method capable of imaging the spatial distribution of superparamagnetic iron oxide particles (SPIO) with high temporal and spatial resolution [1–3]. For spatial encoding, MPI uses a magnetic gradient field providing a field-free point (FFP), which is moved through the hole region of interest. Due to saturation effects, only particles in the close vicinity of the FFP contribute to the signal induced in receive coils. The size of this region, and in turn the sensitivity of MPI, is determined by the magnetic field strength at which the particles reach saturation as well as the gradient strength of the FFP field [4, 5].

Recently, it has been shown that the sensitivity of the method could be significantly improved by using a simultaneous encoding scheme [6]. This can be accomplished by scanning the region of interest with a field-free line (FFL) instead of the field-free point. A comparison of the FFP field and the FFL field is provided in figure 1. For signal encoding, the FFL is rapidly moved back and forth while rotating slowly. Such an encoding scheme requires an assembly capable of rotating and translating the FFL exclusively by varying the applied currents while keeping the setup static in space. Although the Halbach cylinders of order three and higher [7, 8] are known to generate an FFL, they do not allow for rotating the FFL non-mechanically.

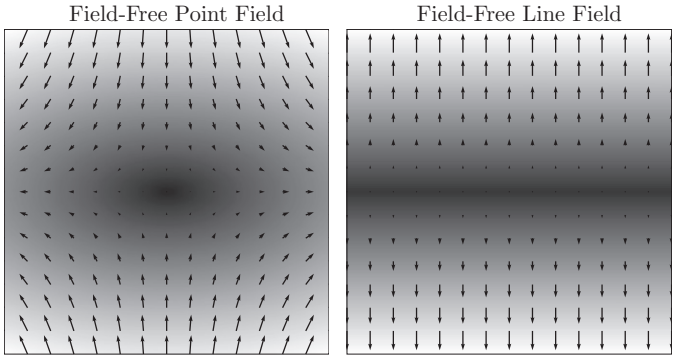

Figure 1. Comparison of an FFP field and an FFL field. Here, black indicates zero field strength and white indicates high field strength.

In [6] the first device was presented, which meets the aforementioned requirements. It consists of 32 electromagnetic coils positioned at equidistant angles on a circle. However, no proof was given that the assembly actually generates an FFL. Moreover, for resistive coils, the suggested scanner requires about 1000 times the electrical power of a conventional FFP scanner of equal size and gradient performance. Because of that, the authors were quite pessimistic about the feasibility of the FFL concept.

The main result of this work is the fact that a rotating FFL can only be generated by three or more Maxwell coil pairs using appropriate currents. To the best of our knowledge, the proof presented here is novel and the problem of generating a rotating FFL was not investigated mathematically to date. Using less than 32 coils significantly improves the efficiency of the coil geometry. We present the first FFL coil assembly for MPI, which is feasible to manufacture requiring for resistive coils roughly the same electrical power as that of an FFP scanner of equal size and gradient performance.

2. Theory

2.1. Preliminaries

Consider a right-handed global Cartesian coordinate system with coordinates $\boldsymbol{r} = (x, y, z)^{\mathsf{T}} = x\boldsymbol{e}_x + y\boldsymbol{e}_y + z\boldsymbol{e}_z \in \mathbb{R}^3$, where $\boldsymbol{e}_x$, $\boldsymbol{e}_y$ and $\boldsymbol{e}_z$ denote the unit vectors in x-, y- and z-directions. To make later derivations more convenient, we introduce a local coordinate system with coordinates $\boldsymbol{r}^\beta$. It is rotated counterclockwise by β within the xy-plane. Thus, three basis vectors are given by $\boldsymbol{e}_x^\beta = (\cos(\beta), \sin(\beta), 0)^{\mathsf{T}}$, $\boldsymbol{e}_y^\beta = (-\sin(\beta), \cos(\beta), 0)^{\mathsf{T}}$ and $\boldsymbol{e}_z^\beta = \boldsymbol{e}_z$. To transform the position of one of both coordinate systems into the other,

$$\boldsymbol{r}^\beta = \boldsymbol{R}^\beta \boldsymbol{r} \tag{1}$$

$$\boldsymbol{r} = \boldsymbol{R}^{-\beta} \boldsymbol{r}^\beta \tag{2}$$

can be used. Here, $\boldsymbol{R}^\beta = \left(\boldsymbol{e}_x^\beta, \boldsymbol{e}_y^\beta, \boldsymbol{e}_z^\beta\right)$ denotes the rotation matrix. Similarly, the magnetic field $\boldsymbol{H}(\boldsymbol{r})$ in global coordinates can be expressed in local coordinates and vice versa by

$$\boldsymbol{H}^\beta(\boldsymbol{r}^\beta) = \boldsymbol{R}^\beta \boldsymbol{H}(\boldsymbol{R}^{-\beta}\boldsymbol{r}^\beta), \tag{3}$$

$$\boldsymbol{H}(\boldsymbol{r}) = \boldsymbol{R}^{-\beta} \boldsymbol{H}^\beta(\boldsymbol{R}^\beta \boldsymbol{r}). \tag{4}$$

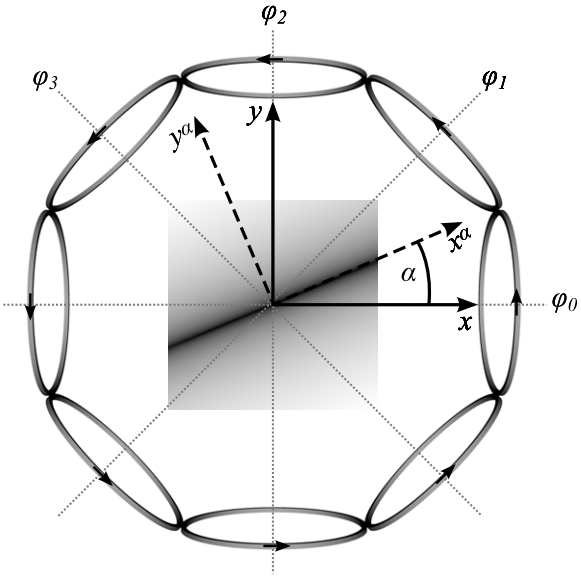

Figure 2. Coil assembly for the generation of a rotating FFL using $L = 4$ Maxwell coil pairs. The current flow of each coil is indicated by arrows and the magnitude of the generated magnetic field is shown as background image.

In the following sections, these relations are used to switch between the global coordinate system, the local coordinate system of the FFL and the local coordinate systems of the Maxwell coil pairs.

2.2. Field-free line field

In this work, FFL generation and rotation in a 2D plane are considered. More precisely, the goal is to generate an FFL in the xy-plane that is orientated along direction $\boldsymbol{d}^{\alpha}_{\mathrm{FFL}} = (\cos\alpha, \sin\alpha, 0)^{\mathsf{T}}$ and crosses the origin. Then, FFL rotation can be easily achieved by varying the angle α. FFL translation is later discussed in section 2.5. In local FFL coordinates $\boldsymbol{r}^{\alpha}$, the rotated FFL field has to fulfill the condition

$$\boldsymbol{H}^{\alpha}(\boldsymbol{r}^{\alpha}) = \boldsymbol{0} \qquad \text{for} \quad \boldsymbol{r}^{\alpha} = (x', 0, 0)^{\mathsf{T}}, \quad x' \in \mathbb{R}. \tag{5}$$

Equivalently, this condition can be formulated in terms of the spatial derivative along the FFL, which has to be zero if we additionally stipulate that the magnetic field is zero at the origin, i.e.

$$\frac{\partial H^{\alpha}_{x}(\boldsymbol{r}^{\alpha})}{\partial \boldsymbol{e}^{\alpha}_{x}} = 0 \qquad \text{for} \quad \boldsymbol{r}^{\alpha} = (x', 0, 0)^{\mathsf{T}}, \quad x' \in \mathbb{R} \tag{6}$$

$$\text{and} \quad \boldsymbol{H}^{\alpha}(\boldsymbol{0}) = \boldsymbol{0}. \tag{7}$$

2.3. Field-free line coil setup

In the following, we describe how the coil assembly is used to generate and rotate a magnetic FFL. It consists of $2L$ coils ($L \geqslant 3$) that are positioned at equidistant angles $\varphi_l = \pi \frac{l}{L}$ on a circle of diameter d_{tube}. The coils point toward the center, as it is illustrated in figure 2. Each

pair of opposing coils is arranged in Maxwell configuration [9] and driven by current flowing in converse direction. The Maxwell coil pairs generate a constant gradient field with an FFP at the center of the coordinate system. In rotated coordinates $\boldsymbol{r}^{\varphi_l}$, the magnetic field of the lth Maxwell coil pair is approximatively given by

$$\boldsymbol{H}_l^{\varphi_l}(\boldsymbol{r}^{\varphi_l}) = I_l S \begin{pmatrix} 2 & 0 & 0 \\ 0 & -1 & 0 \\ 0 & 0 & -1 \end{pmatrix} \boldsymbol{r}^{\varphi_l} = I_l \boldsymbol{G} \boldsymbol{r}^{\varphi_l}. \tag{8}$$

Here, I_l is the current flowing through the coil pair and S is a factor determined by the coil geometry. The field (8) represents the ideal magnetic gradient field, which is exactly generated when the coils have infinite distance and diameter. In this section, we assume that the coils fulfill these properties. For finite distance and diameter, the approximation is only valid in a certain region at the center between both coils. Therefore, the FFL is expected to be accurate only in a certain region as well, which is investigated in section 3. In global coordinates, the field (8) is given by

$$\boldsymbol{H}_l(\boldsymbol{r}) = \boldsymbol{R}^{-\varphi_l} \boldsymbol{H}_l^{\varphi_l}(\boldsymbol{R}^{\varphi_l} \boldsymbol{r}) = I_l \boldsymbol{R}^{-\varphi_l} \boldsymbol{G} \boldsymbol{R}^{\varphi_l} \boldsymbol{r} = I_l \boldsymbol{G}^{\varphi_l} \boldsymbol{r},$$

where

$$\boldsymbol{G}^{\varphi_l} = S \begin{pmatrix} \frac{1}{2} + \frac{3}{2}\cos(2\varphi_l) & -\frac{3}{2}\sin(2\varphi_l) & 0 \\ -\frac{3}{2}\sin(2\varphi_l) & \frac{1}{2} - \frac{3}{2}\cos(2\varphi_l) & 0 \\ 0 & 0 & -1 \end{pmatrix}. \tag{9}$$

In FFL-coordinates $\boldsymbol{r}^{\alpha}$, this field can be expressed as

$$\boldsymbol{H}_l^{\alpha}(\boldsymbol{r}^{\alpha}) = I_l \boldsymbol{G}^{\varphi_l - \alpha} \boldsymbol{r}^{\alpha}.$$

Finally, to obtain the magnetic field generated by the complete coil assembly, the superposition of the magnetic fields $\boldsymbol{H}_l^{\alpha}(\boldsymbol{r}^{\alpha})$ is computed yielding

$$\boldsymbol{H}^{\alpha}(\boldsymbol{r}^{\alpha}) = \sum_{l=0}^{L-1} I_l \boldsymbol{G}^{\varphi_l - \alpha} \boldsymbol{r}^{\alpha} = \boldsymbol{D}^{\alpha} \boldsymbol{r}^{\alpha}, \tag{10}$$

with

$$\boldsymbol{D}^{\alpha} = S \begin{pmatrix} \sum_{l=0}^{L-1} I_l \left(\frac{1}{2} + \frac{3}{2}\cos(2\varphi_l - 2\alpha)\right) & -\sum_{l=0}^{L-1} I_l \frac{3}{2}\sin(2\varphi_l - 2\alpha) & 0 \\ -\sum_{l=0}^{L-1} I_l \frac{3}{2}\sin(2\varphi_l - 2\alpha) & \sum_{l=0}^{L-1} I_l \left(\frac{1}{2} - \frac{3}{2}\cos(2\varphi_l - 2\alpha)\right) & 0 \\ 0 & 0 & -\sum_{l=0}^{L-1} I_l \end{pmatrix}. \tag{11}$$

2.4. Field-free line generation

To generate an FFL with the described coil assembly, the currents have to be chosen appropriately. Weizenecker *et al* [6] proposed to use

$$I_l = \tilde{A}\sin^2(\varphi_l - \alpha) + \tilde{C} = \frac{\tilde{A}}{2}(1 - \cos(2\varphi_l - 2\alpha)) + \tilde{C}, \tag{12}$$

without giving a rule how to select the parameters $\tilde{A}$ and $\tilde{C}$. For convenience, we introduce $A = \frac{\tilde{A}}{2}$ and $\gamma = 1 + \frac{2\tilde{C}}{\tilde{A}}$ and express the currents as $I_l = A(\gamma - \cos(2\varphi_l - 2\alpha))$. Now, we can state our main result.

Theorem 1. *The superposition of $L \geqslant 3$ ideal gradient fields rotated by equidistant angles $\varphi_l = \pi \frac{l}{L}$ generates a field-free line in the xy-plane through the center along direction $\boldsymbol{d}^{\alpha}_{\mathrm{FFL}}$ for currents $I_l = A(\gamma - \cos(2\varphi_l - 2\alpha))$ with $\gamma = \frac{3}{2}$.*

In order to prove the theorem, we need following lemma:

Lemma 1. *Let $L \geqslant 3$, $\alpha \in \mathbb{R}$ and $q \in \{1, 2\}$ be given, then*

$$\sum_{l=0}^{L-1} \cos\left(2q\pi \frac{l}{L} + 2q\alpha\right) = 0. \tag{13}$$

Proof of lemma 1. The result follows as a special case of the summation of the complex roots of unity. It is well known that for $L \in \mathbb{N}$ and $k = 1, \ldots, L-1$

$$\sum_{l=0}^{L-1} \exp\left(2\pi \mathrm{i} \frac{kl}{L}\right) = 0.$$

By using the Eulers relation $\exp(\mathrm{i}\alpha) = \cos(\alpha) + \mathrm{i}\sin(\alpha)$ and taking the real and imaginary part of the sum one obtains

$$\sum_{l=0}^{L-1} \cos\left(2\pi \frac{kl}{L}\right) = \sum_{l=0}^{L-1} \sin\left(2\pi \frac{kl}{L}\right) = 0.$$

Now, weight the cosine sum with $\cos(2q\alpha)$ and the sine sum with $\sin(2q\alpha)$ and subtract both sums from each other to obtain

$$\sum_{l=0}^{L-1} \cos(2q\alpha) \cos\left(2\pi \frac{kl}{L}\right) - \sin(2q\alpha) \sin\left(2\pi \frac{kl}{L}\right) = 0.$$

Using the trigonometric addition theorem $\cos(a + b) = \cos(a)\cos(b) - \sin(a)\sin(b)$ and $k = q$ completes the proof of lemma 1. □

Proof of theorem 1. Recall the FFL conditions stated in (6) and (7). Obviously, it holds that $\boldsymbol{H}^{\alpha}(\boldsymbol{0}) = \boldsymbol{D}^{\alpha}\boldsymbol{0} = \boldsymbol{0}$. Thus, it remains to be shown that

$$\frac{\partial H^{\alpha}_x(\boldsymbol{r}^{\alpha})}{\partial \boldsymbol{e}^{\alpha}_x} = 0.$$

The spatial derivative along the FFL is the upper left component of the 3×3 matrix $\boldsymbol{D}^{\alpha}$ given in (11). Hence, we obtain

$$\frac{\partial H^{\alpha}_x(\boldsymbol{r}^{\alpha})}{\partial \boldsymbol{e}^{\alpha}_x} = AS \sum_{l=0}^{L-1} (\gamma - \cos(2\varphi_l - 2\alpha)) \left(\frac{1}{2} + \frac{3}{2}\cos(2\varphi_l - 2\alpha)\right).$$

By expanding the brackets and using the trigonometric formula $\cos^2(a) = \frac{1}{2} + \frac{1}{2}\cos(2a)$ we derive

$$\frac{\partial H^{\alpha}_x(\boldsymbol{r}^{\alpha})}{\partial \boldsymbol{e}^{\alpha}_x} = AS\left[L\left(\frac{1}{2}\gamma - \frac{3}{4}\right) + \left(\frac{3}{2}\gamma - \frac{1}{2}\right)\sum_{l=0}^{L-1}\cos(2\varphi_l - 2\alpha) + \frac{3}{4}\sum_{l=0}^{L-1}\cos(4\varphi_l - 4\alpha)\right].$$

Due to lemma 1, both sums vanish for $L \geqslant 3$ yielding

$$\frac{\partial H^{\alpha}_x(\boldsymbol{r}^{\alpha})}{\partial \boldsymbol{e}^{\alpha}_x} = ASL\left(\frac{1}{2}\gamma - \frac{3}{4}\right). \tag{14}$$

Hence, the spatial derivative along the FFL is zero for $\gamma = \frac{3}{2}$ yielding the proposition of theorem 1. □

In a similar way, the gradient strength in perpendicular directions to the FFL can be computed yielding

$$\frac{\partial H_y^\alpha(\boldsymbol{r}^\alpha)}{\partial \boldsymbol{e}_y^\alpha} = -\frac{\partial H_z^\alpha(\boldsymbol{r}^\alpha)}{\partial \boldsymbol{e}_z^\alpha} = ASL\frac{3}{2}. \tag{15}$$

To achieve a certain gradient strength G, the current parameter A has to be chosen as

$$A = \frac{2}{3}\frac{G}{SL}. \tag{16}$$

2.5. Field-free line translation

For translating the FFL, three Helmholtz coil pairs can be used, which are orientated in x-, y- and z-directions (not shown in figure 2). In x- and y-directions, it is possible to share the same coils for generating and translating the FFL by superposition of the currents in the respective coils. Each of the Helmholtz coil pairs generates a homogeneous magnetic field, ideally given by

$$\boldsymbol{H}_x(\boldsymbol{r}) = I_x S_x \boldsymbol{e}_x, \tag{17}$$

$$\boldsymbol{H}_y(\boldsymbol{r}) = I_y S_y \boldsymbol{e}_y, \tag{18}$$

$$\boldsymbol{H}_z(\boldsymbol{r}) = I_z S_z \boldsymbol{e}_z. \tag{19}$$

The superposition

$$\boldsymbol{H}_{\text{trans}} = (I_x S_x, I_y S_y, I_z S_z)^{\mathsf{T}} \tag{20}$$

allows for generating a homogeneous field in any direction in space.

Lemma 2. *The FFL generated by the superposition of $L \geqslant 3$ ideal gradient fields can be translated to position $\boldsymbol{t} = (t_x, t_y, t_z)^{\mathsf{T}} \in \mathbb{R}^3$ using a homogeneous translation field $\boldsymbol{H}_{\text{trans}} = -\boldsymbol{H}^\alpha(\boldsymbol{t})$.*

Proof of lemma 2. At position $\boldsymbol{t}$, the rotated FFL field is given by $\boldsymbol{H}^\alpha(\boldsymbol{t})$. For translating the FFL to position $\boldsymbol{t}$, the total magnetic field $\boldsymbol{H}$ at this very point has to be canceled out, i.e.

$$\boldsymbol{H}(\boldsymbol{t}) = \boldsymbol{H}^\alpha(\boldsymbol{t}) + \boldsymbol{H}_{\text{trans}} = \boldsymbol{0}.$$

Thus, the direction of the translation field has to be

$$\boldsymbol{H}_{\text{trans}} = -\boldsymbol{H}^\alpha(\boldsymbol{t}).$$

As the spatial derivative is not affected by the homogeneous field, it remains zero in direction $\boldsymbol{d}_{\text{FFL}}^\alpha$. Thus, an FFL is established that crosses point $\boldsymbol{t}$ and is orientated along $\boldsymbol{d}_{\text{FFL}}^\alpha$. □

3. Simulation

Next, we leave the assumption of idealized gradient fields and turn toward the magnetic field actually generated by the coil setup. Then, the magnetic field of each Maxwell coil pair is linear only for the high symmetric point and deviates in radial direction from the ideal case.

In order to examine the accuracy of the FFL for real magnetic fields, simulations are carried out using numerical evaluation of the Biot–Savart law [10]. Different numbers of Maxwell coil pairs $L = 3, 4, 8, 16$ and a circle diameter of $d_{\text{tube}} = 0.5$ m are used. The

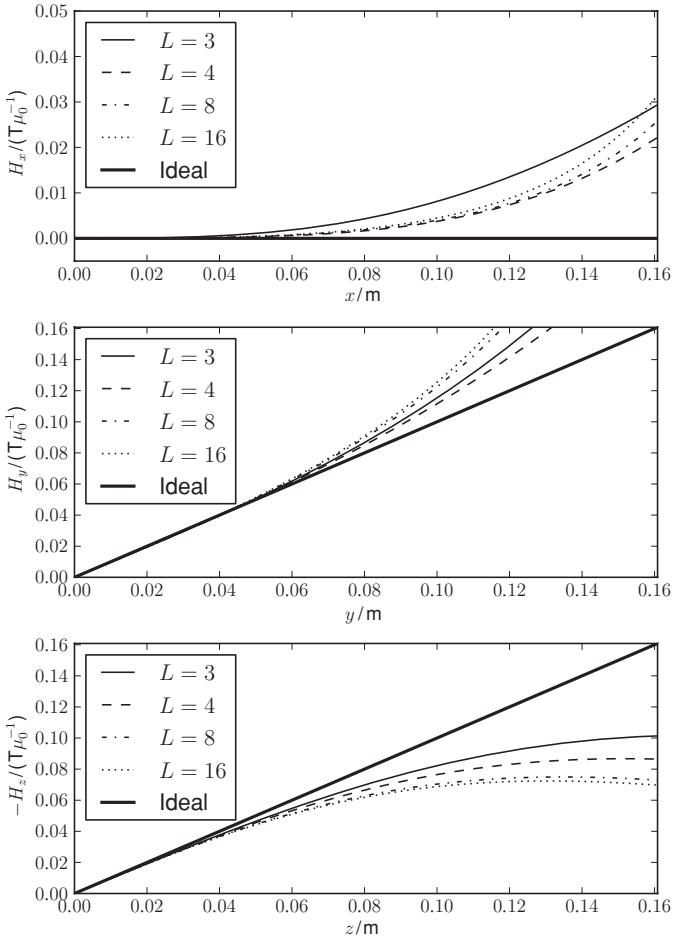

Figure 3. Simulated magnetic fields in x-, y- and z-directions in coordinates of the rotated FFL for different numbers of Maxwell coil pairs. Shown are the first 0.16 m of the 0.25 m circle radius, on which the coils are located.

diameter of each coil is chosen as large as possible without intersecting the neighboring coils, i.e. $d_L = d_{\text{tube}} \tan \frac{\pi}{2L}$. Consequently, the size of the coils, and in turn the sensitivity S, decreases with increasing L. Further, for fair comparison of the electrical power loss, the coils have a cross-section, which is proportional to the square of the coil diameter d_L. Hence, the coil resistance is inversely proportional to d_L. The current parameter is adapted to generate a gradient strength of 1.0 $\mathrm{Tm}^{-1}\mu_0^{-1}$ perpendicular to the FFL at the center.

The quality of the resulting fields is illustrated in figure 3. For each L, the angle α_L is chosen such that the FFL is located in-between the symmetry axes of two subsequent coils, i.e. $\alpha_L = \frac{\pi}{2L}$. At this angle, the quality of the FFL is found to be worst. As it can be seen, the best FFL, and the most constant gradient in y-direction, is obtained for $L = 4$. In the z-direction, $L = 3$ results in the most constant gradient.

For power loss considerations, the required electrical power of the FFL coil setup is compared to that of a Maxwell coil pair generating an FFP field with 1.0 $\mathrm{Tm}^{-1}\mu_0^{-1}$ gradient strength in x-direction and half of this value in y- and z-directions. The resulting numbers are

Table 1. Electrical power loss of FFL setups using different coil pair numbers L. The numbers are given relative to the electrical power loss of an FFP scanner of equal size and gradient performance.

L	3	4	8	16
$P_L^{\mathrm{FFL}}/P^{\mathrm{FFP}}$	3.3	6.9	74.4	1081.2

listed in table 1. As can be seen, less coils do not only provide a better field but are additionally considerably more efficient.

4. Conclusion

In conclusion, we have proven that a magnetic field-free line can be established at an arbitrary direction in a 2D plane by only three Maxwell coil pairs. In simulations of real coil setups, the optimal number of Maxwell coil pairs of the presented setup was found to be 3 or 4 depending on whether it is the power loss or the quality of the generated magnetic field, which should be optimized. Here, a certain coil geometry was considered, for which the coil size decreases with the total number of coils used. It might be possible to further optimize the coil configuration by using overlapping coils.

Using the proposed FFL setups for imaging with MPI allows us to determine the line integrals of the particle concentration along the FFL. Therefore, the object is sampled in the Radon space [11], so that one can think of applying reconstruction algorithms commonly used in computed tomography [12].

The drastically reduced power consumption compared to the coil assembly proposed by Weizenecker *et al* [6] denotes a major step for the feasibility of the FFL geometry and, due to the improved sensitivity, for MPI in general. However, the concept of a field-free line is not necessarily tied to MPI and might find its application in other fields as well.

5. Acknowledgment

We would like to thank Bernhard Gleich (Philips Technologie GmbH Forschungslaboratorien, Hamburg, Germany) for numerous enlightening discussions on the presented subject that have improved the communication.

References

[1] Gleich B and Weizenecker J 2005 Tomographic imaging using the nonlinear response of magnetic particles *Nature* **435** 1214–7
[2] Sattel T F, Knopp T, Biederer S, Gleich B, Weizenecker J, Borgert J and Buzug T M 2009 Single-sided device for magnetic particle imaging. *J. Phys. D: Appl. Phys.* **42** 1–5
[3] Weizenecker J, Gleich B, Rahmer J, Dahnke H and Borgert J 2009 Three-dimensional real-time *in vivo* magnetic particle imaging. *Phys. Med. Biol.* **54** L1–L10
[4] Weizenecker J, Borgert J and Gleich B 2007 A simulation study on the resolution and sensitivity of magnetic particle imaging. *Phys. Med. Biol.* **52** 6363–74
[5] Knopp T, Biederer S, Sattel T, Weizenecker J, Gleich B, Borgert J and Buzug T M 2009 Trajectory analysis for magnetic particle imaging. *Phys. Med. Biol.* **54** 385–97
[6] Weizenecker J, Gleich B and Borgert J 2008 Magnetic particle imaging using a field free line. *J. Phys. D: Appl. Phys.* **41** 3 pp
[7] Halbach K 1980 Design of permanent multipole magnets with oriented rare earth cobalt material. *Nucl. Instrum. Methods* **169** 1–10

[8] Halbach K 1985 Application of permanent magnets in accelerators and electron storage rings. *J. Appl. Phys.* **57** 3605
[9] Maxwell J C 1873 *A Treatise on Electricity and Magnetism* (Oxford: Clarendon)
[10] Jackson J D 1999 *Classical Electrodynamics* (New York: Wiley)
[11] Radon J H 1917 Über die Bestimmung von Funktionen durch Ihre Integralwerte längs gewisser Mannigfaltigkeiten *Berichte der Sächsischen Akadamie der Wissenschaft* **69** 262–77
[12] Buzug T M 2008 *Computed Tomography: From Photon Statistics to Modern Cone-Beam CT* (Berlin: Springer-Verlag)